

# **A single element imaging spectrograph**

Daniel M. Cotton, Timothy Cook, and Supriya Chakrabarti

Earth and Planetary Atmospheres Group

Center for Space Physics

Boston University, Boston, MA 02215

(617) 353-7431

## **Abstract**

We briefly describe a spectrograph concept designed for both high wavelength and high spatial resolution (in one dimension). We refer to the design as a Single Element Imaging Spectrograph (SEIS). It is a one bounce diffractive system which combines the spectral properties of a Rowland mount spectrograph with the imaging (spatial resolution) properties of a Wadsworth through the use of a toroidal diffraction grating. No primary optics are necessary, making the system especially attractive for use in the extreme and far ultraviolet (EUV and FUV) where low reflectivity of common optical coatings can severely limit instrument sensitivity.

## **Key Words**

Ultraviolet, Grating Spectrograph

## 1. Introduction

Instruments that can analyze extended extreme ultraviolet (EUV) and far ultraviolet (FUV) emission sources spatially and spectrally are important tools in many fields of physics: astrophysics, planetary atmospheres, plasma physics, aeronomy, etc. Thus, scientists in these fields take a particular interest in the development of imaging spectrographs.

Typically, such instruments are limited to only one or two optical components, since low reflectivities and transmissions of common optical components in this spectral range (wavelength,  $\lambda \lesssim 2000 \text{ \AA}$ ) make it highly desirable to minimize the number of reflections or transmissions. This is especially true in the EUV (wavelength,  $\lambda \lesssim 1000 \text{ \AA}$ ) where transmissive optical components are nonexistent and normal incidence reflectivities are low. Grazing incidence optics play a large role in EUV instruments, due to their generally higher throughput. However, there are limitations to the imaging of grazing incidence optics, due to aberrations and figure errors. Although grazing incidence systems are definitely useful in some applications, in this paper, for brevity, we will concentrate only on the normal incidence systems.

The conventional types of single element, normal incident spectrographs that are used to study EUV sources are the Rowland <sup>1, 2</sup> and Wadsworth mount <sup>3</sup> spectrographs. The Rowland mount spectrograph is a compact simple instrument with a large field of view. However, it has no imaging capabilities on its own; imaging using a Rowland is usually accomplished by using fore optics (e.g. an off axis paraboloid <sup>4</sup>). This introduces more scattered light into the system and, more importantly, makes it less sensitive in the EUV. Furthermore, it becomes larger and heavier, and both of these aspects are undesirable in space flight applications. The Wadsworth mount on the other hand, images in one dimension. However, a collimator is used to narrow the field of view in the dispersion direction in order to define the spectral resolution.

In this paper, we describe a new spectrograph concept which combines the simplicity and large field of view of the Rowland mount with the imaging of a Wadsworth by means of a toroidal diffraction grating. We call this system,

the Single Element Imaging Spectrograph (SEIS). In the following two sections, some of its properties are described by using two examples in which the SEIS has definite advantages over its Rowland and Wadsworth counterparts.

## 2. Optical Design

The SEIS optical configuration is nearly identical to the Rowland mount spectrograph<sup>5</sup> (see Figure 1). As with the Rowland, the radius of curvature of the grating in the dispersion plane is the diameter of the Rowland circle, i.e. for a slit on this circle the focal plane is just the Rowland cylinder, and the spectrum can be located through the use of the grating equation:

$$\sin\beta = \sin\alpha + m\lambda/d \quad (1)$$

where  $\lambda$  is the wavelength,  $\alpha$  is the angle of incidence,  $d$  is the groove spacing on the grating, and  $\beta$  is the diffracted angle. In this plane (represented by the page of Figure 1), the spectrograph acts essentially as a Rowland. For example, the width of the slit in some cases defines the spectral resolution of the SEIS system as in the case of the Rowland mount, and the field of view (FOV) can be made fairly large ( $10^\circ$  or larger) in the dispersion direction.

Out of this plane, there are a few significant differences between the SEIS and the Rowland. For one, the slit can be much longer than its Rowland counterpart. This is similar to the Wadsworth in which the entrance aperture is approximately the same size as the grating. With the SEIS, there is a trade-off between the length of the slit and the spectral resolution as with the Rowland, but in general, one can easily double the slit height of a Rowland spectrograph with the same FOV and still achieve comparable spectral resolution. Another unique property of the SEIS is that the FOV in the imaging direction can be, for all practical purposes, unlimited. For normal incidence systems, it can be large ( $\sim 10^\circ$ ) without a significant loss in imaging quality depending upon the slit length. However, there is a degradation of spectral resolution off axis. This trade-off between grasp (collecting area  $\times$  field of view) and spectral and spatial resolution is taken into account when one is designing for a specific application. In comparison with the Rowland and Wadsworth, the SEIS offers more degrees of freedom in designing for specific applications.

Intuitively and practically, the SEIS can be thought of as a hybrid of the Rowland and Wadsworth. It acts as a Rowland in the dispersion direction and a Wadsworth in the imaging direction. The key to this hybridization is the use of a toroidal grating with the radius of curvature of an equivalent Rowland (diameter of the Rowland circle) in the dispersion plane and a radius of curvature of a Wadsworth in the imaging plane (approximately twice the diameter of the Rowland circle). Note that this is unlike a conventional toroidal grating spectrograph in which the sagittal radius is chosen to make the image of the slit stigmatic for a particular wavelength. Here, the toroid is used to image objects at infinity onto the focal plane.

### 3. Optical Properties

In this section, we present some of the properties of the SEIS and then illustrate them using two practical examples. Figure 2 shows the geometry and denotes the coordinates of the torus grating. Our formulation of SEIS's optical properties will follow that of Haber<sup>6</sup> who patterned his analysis after Beutler<sup>5</sup>. Briefly stated, it is based upon Fermat's principle; the condition of focus is that the light path function (the distance from the slit at A to the grating at an arbitrary point, P, and then to the focal point B or  $F = AP + PB + y\lambda/d$  (illustrated in Figure 2) is an extreme with respect to the point at which a ray hits the grating (P). In other words,  $dF/dP = 0$ . Deviations from this condition yield the aberrations of the focus that determine the imaging and spectral resolution of the system. For more details, see *Beutler*<sup>5</sup>.

As with the Rowland, the condition for  $dF/dy = 0$  for the 0th and 1st order terms yields the grating equation (Eq. 1) and the Rowland circle condition:

$$ra = R\cos(\alpha) \ ; \ rb = R\cos(\beta) \tag{2}$$

Note that we obtain the Rowland condition rather than the Wadsworth condition, since we are assuming that the source is defined by the slit in the y direction.

However, in the  $z$  direction we are imaging points located at infinity (e.g. the sky). Therefore, by setting  $ra = \infty$  in equation 28 of *Haber*<sup>6</sup>, the condition to eliminate the primary astigmatism for a particular wavelength becomes

$$\rho/R = \cos\beta(\cos\alpha + \cos\beta) \quad (3)$$

where  $\rho$  is the radius of curvature of the grating in the  $xz$  plane and  $R$  is the radius of curvature in the  $xy$  plane (see Figure 2).

Astigmatism,  $As$ , for other wavelengths can be calculated using the speed of the beam in the imaging direction,  $L/r_{bh}$ , and the distance between the Rowland circle and the position at which the beam is stigmatic,  $s = r_{bh} - R\cos\beta$ . Here,  $r_{bh}$  is the distance from the center of the grating to the horizontal stigmatic point,  $L$  is the length of the illuminated rulings on the grating, and  $R\cos\beta$  is the distance to the Rowland circle from the center of the grating. In other words,

$$As = sL/r_{bh} = \frac{L}{\rho}[\rho - R\cos\beta(\cos\alpha + \cos\beta)] \quad (4)$$

For small  $\alpha$  and  $\beta$ , as in the case of normal incidence, the primary astigmatism will scale with  $\beta\Delta\beta + \alpha\Delta\alpha$ .

The first example we have selected to illustrate the SEIS properties derived above is a solar EUV spectrograph with parameters comparable to those currently used<sup>7</sup>. Figure 1 is a diagram of the optical layout of the instrument. It was designed to measure the solar EUV flux between 300 and 1300 Å at about 10 Å (FWHM) resolution and to spatially resolve the solar disk in one dimension with a resolution of .05° (FWHM) (about one tenth of the disk). The grating for the SEIS mount has a .2 meter radius of curvature in the dispersion direction and a 399.13 mm radius in the imaging direction, a line density of 850/mm, and an active area of 8.8 × 9.7 mm to accommodate its 2.5° × 2.5° field-of-view. The slit length was made short (1 mm) to minimize the astigmatism away from the corrected line, 800 Å. The parameters of the instrument are listed in Table 1.

Figure 3 is a raytrace of the solar SEIS system shown in Figure 3. Three arbitrary doublets (9.4 Å apart) at 300, 800, and 1300 Å were traced for 50 different angles in the imaging plane. A blowup of the raytrace shown in Figure 4

reveals that the lines are clearly resolved and the imaging resolution is  $.4''$  full-width at half-maximum (FWHM) making it basically diffraction limited. We could easily increase the grasp by an order of magnitude by elongating the slit and grating by a centimeter with a loss of imaging to  $9''$  (still well within the  $3'$  design specifications) due to astigmatism (away from the corrected wavelength) and coma. However, since the target is so bright, this is not necessary.

The second example is a lightweight ( $< 5$  kg) EUV instrument designed for planetary missions. It is fashioned after part of the *Cassini UVS* <sup>8</sup> that we used as a benchmark. It is similar to the solar instrument with some differences: it is slightly larger and, with a  $300 \times 600$  mm radii toroidal grating, has a bandpass of 500–1150Å with about 2Å spectral resolution, and has an imaging capability of  $1.2'$ . The major difference is that it has a long slit (35 mm) to achieve higher sensitivity. The instrument is summarized in Table 1. Figures ??–8 show raytraces for the planetary design. The instrument matches the predicted performance of the *Cassini UVS* spectral (2–5Å) and spatial ( $0.028^\circ$ ) resolution. Also, while the *Cassini UVS* has a much larger geometric collecting area than the SEIS, this instrument's wider FOV compensates to give this design a similar geometric grasp. The SEIS, however, has only one reflection, so it can achieve a larger sensitivity. Furthermore, it is smaller and thus lighter, which is very important in this type of application.

Although both the solar and planetary designs have good response in both the dispersion and imaging directions, the solar spectrograph has much better spatial resolution while the planetary instrument has better spectral resolution. This can be attributed to the differences in the slit geometriess and  $f/\#s$  between the two. Both instruments have slit-limited spectral resolutions; the solar instrument with the lower dispersion and wider slits has lower spectral resolution than the planetary instrument. The image quality difference can be attributed to the difference in the  $f/\#s$  of the two spectrographs in the imaging direction. As with the Rowland and Wadsworth spectrographs, the aberrations increase with the speed of the SEIS. This is reflected in the difference between the solar SEIS, which is slower with better imaging quality, and the planetary SEIS, which is faster and has poorer imaging quality. We have also observed similar increases in the aberrations when  $\alpha$  and  $\beta$  are increased. Not unsurprisingly then, the SEIS coma, astigmatism, and curvature properties appear very similar to those of the Rowland and Wadsworth

spectrographs.

#### **4. Conclusion**

We have presented a new spectrograph design that combines the properties of the conventional one-bounce concave grating systems, the Rowland and Wadsworth mounts. The single element imaging spectrograph allows for high resolution in the spatial and imaging directions.

#### **5. Acknowledgements**

This work was supported by NASA grants NAG5-657 and NAG5-646.

## References

1. S. Kumar, F. Paresce, S. Bowyer and M. Lampton, "Extreme Ultraviolet Spectrometer for Space Research,," *Appl. Opt.* **13**, 575-580 (1974).
2. S. Bowyer, R. Kimble, F. Paresce, M. Lampton and G. Penegor, "Continuous-readout extreme-ultraviolet airglow spectrometer," *Appl. Opt.* **20**, 477-486 (1981).
3. A. B. Christensen, D. C. Kayser, J. B. Pranke, P. R. Straus, D. J. Gueierrez, S. Chakrabarti, R. P. McCoy, R. R. Meier, K. D. Wolfram, and J. M. Picone, "Instrumentation on the RAIDS Experiment II: Extreme Ultraviolet Spectrometer, Photometer, and NEAR-IR Spectrometer," *Proc. SPIE* **1745**, 89-98 (1992).
4. C. Martin and S. Bowyer, "Discovery of High Ionization Far Ultraviolet Line Emission from the Interstellar Medium," *Astrophys. J.* **350**, 242-261 (1990).
5. H. G. Beutler, "The Theory of the Concave Grating," *J. Opt. Soc. Am.* **35**, 311-350 (1945).
6. H. Haber, "The Torus Grating," *J. Opt. Soc. Am.* **40**, 153-165 (1950).
7. T. N. Woods and G. J. Rottman, "Solar EUV Irradiance Derived From a Sounding Rocket Experiment on November 10, 1988," *J. Geophys. Res.* **95**, 6227-6236 (1990).
8. W. E. McClintock, G. M. Lawrence, R. A. Kohnert and L. W. Esposito, "Optical Design of the Ultraviolet Imaging Spectrograph for the Cassini Mission to Saturn," *Proc. SPIE* **1745**, 26-38 (1992).

## List of Figures

1	The optical layout of the SEIS mount spectrograph. . . . .	10
2	Illustration of the coordinates for the toroidal grating. This diagram is fashioned after Figure 2 of <i>Haber</i> <sup>6</sup> . . . . .	11
3	A raytrace for the SEIS solar spectrograph system described in the text. Three arbitrary doublet separated by 9.4 Å were traced at 300, 800 and 1300 Å for 50 discrete angular positions between -1.25 and 1.25° along the slit. . . . .	12
4	A blowup of the raytrace showing the wavelength and imaging resolution in more detail. . . . .	13
5	efficiency . . . . .	14
6	The instrument . . . . .	15
7	The instrument . . . . .	16
8	The instrument . . . . .	17

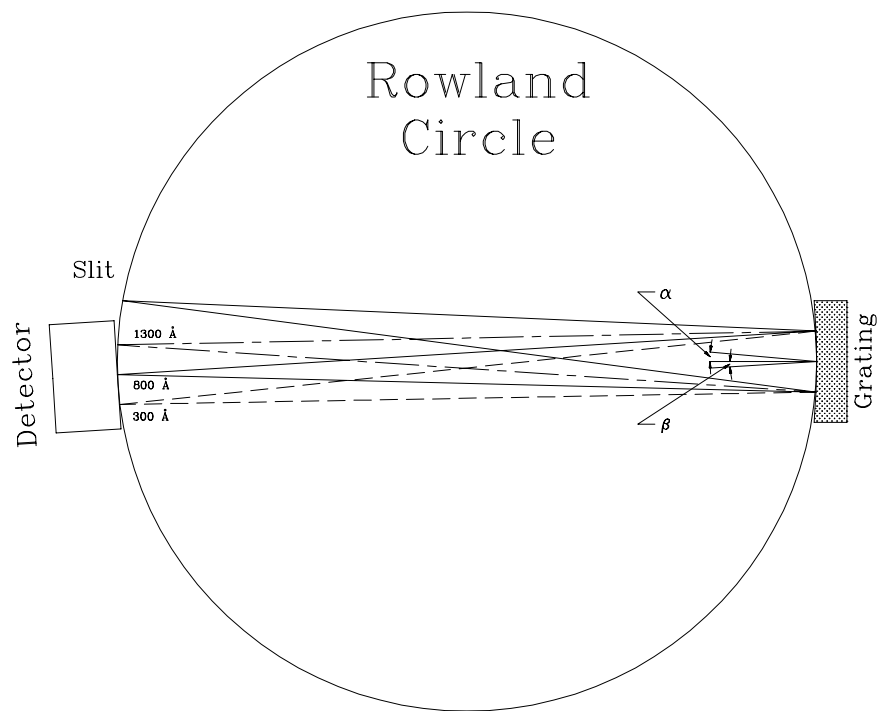


Fig. 1. The optical layout of the SEIS mount spectrograph.

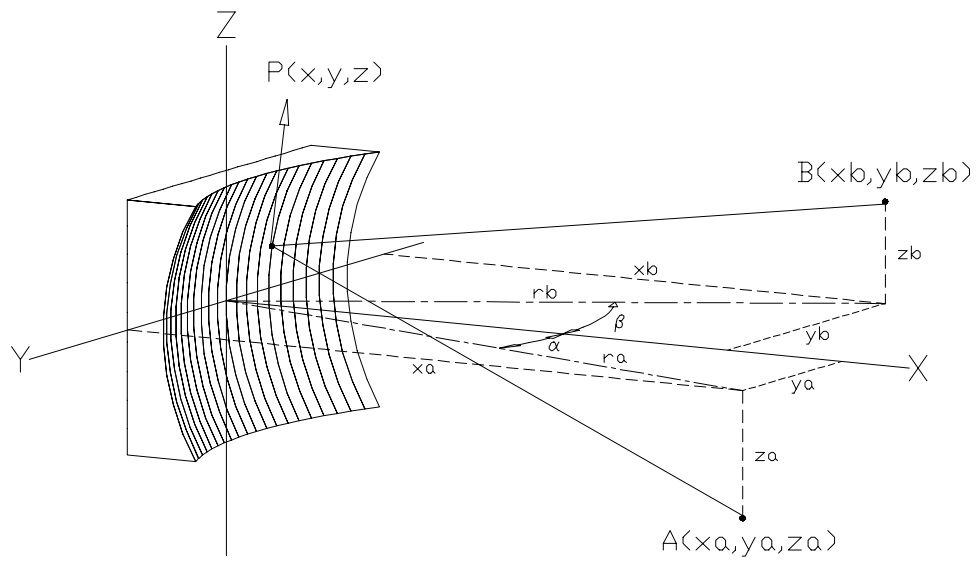


Fig. 2. Illustration of the coordinates for the toroidal grating. This diagram is fashioned after Figure 2 of *Haber*<sup>6</sup>

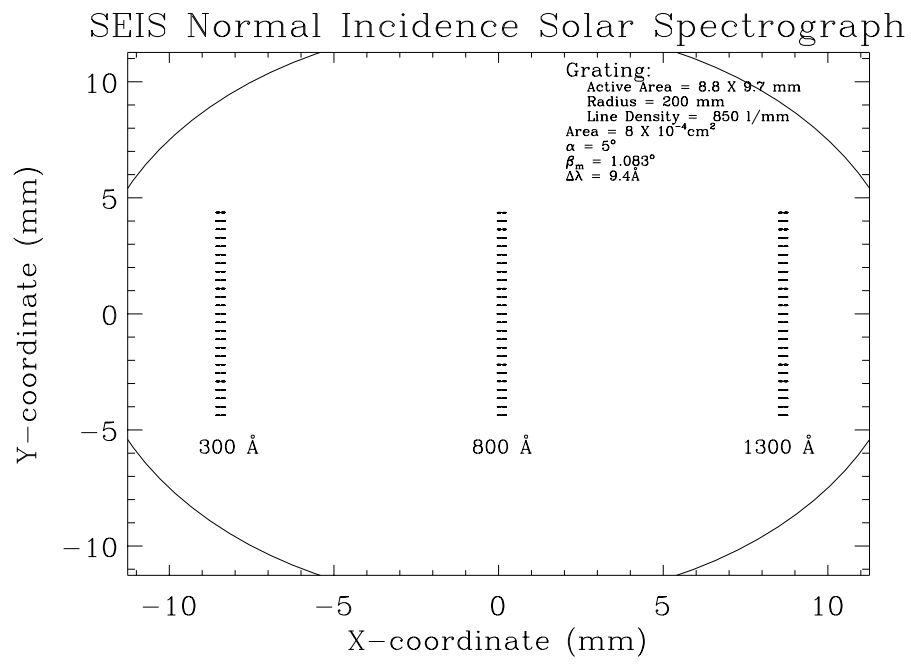


Fig. 3. A raytrace for the SEIS solar spectrograph system described in the text. Three arbitrary doublet separated by  $9.4 \text{ \AA}$  were traced at 300, 800 and 1300  $\text{\AA}$  for 50 discrete angular positions between  $-1.25$  and  $1.25^\circ$  along the slit.

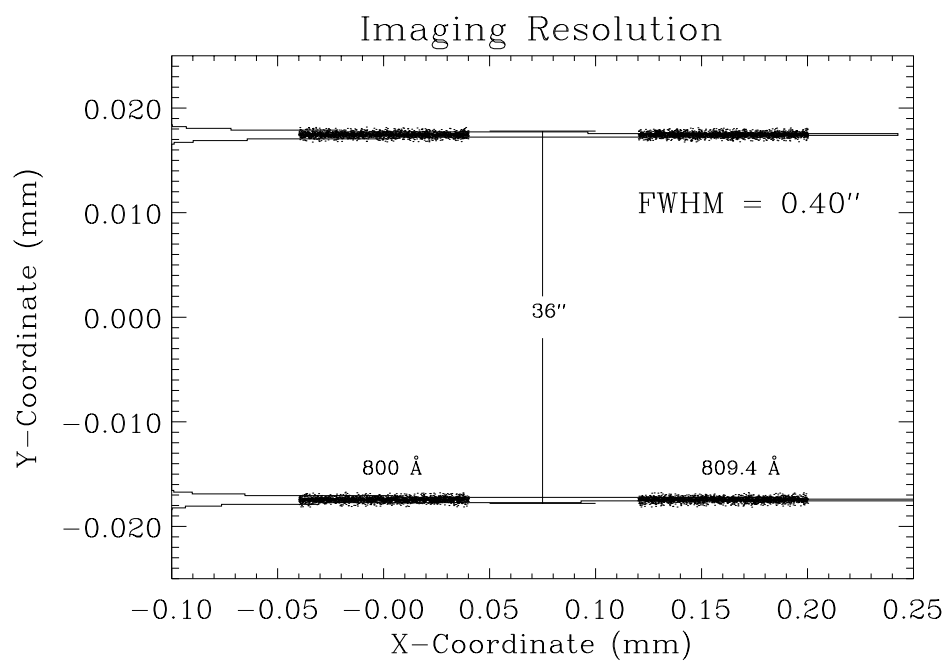


Fig. 4. A blowup of the raytrace showing the wavelength and imaging resolution in more detail.

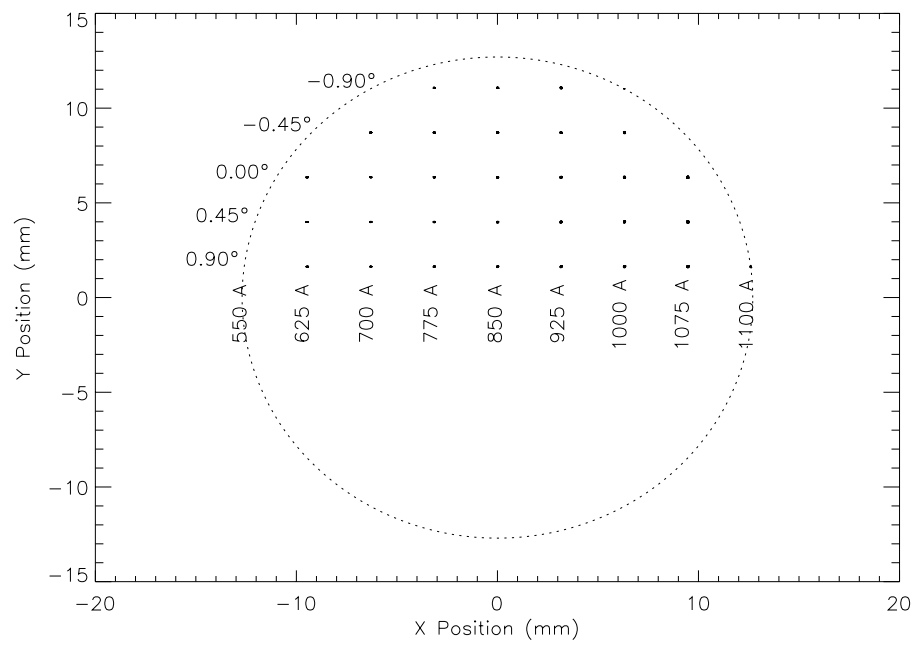


Fig. 5. Simulated planetary SEIS detector image. The instrument uses only half of the detector; the other half is reserved for another instrument.

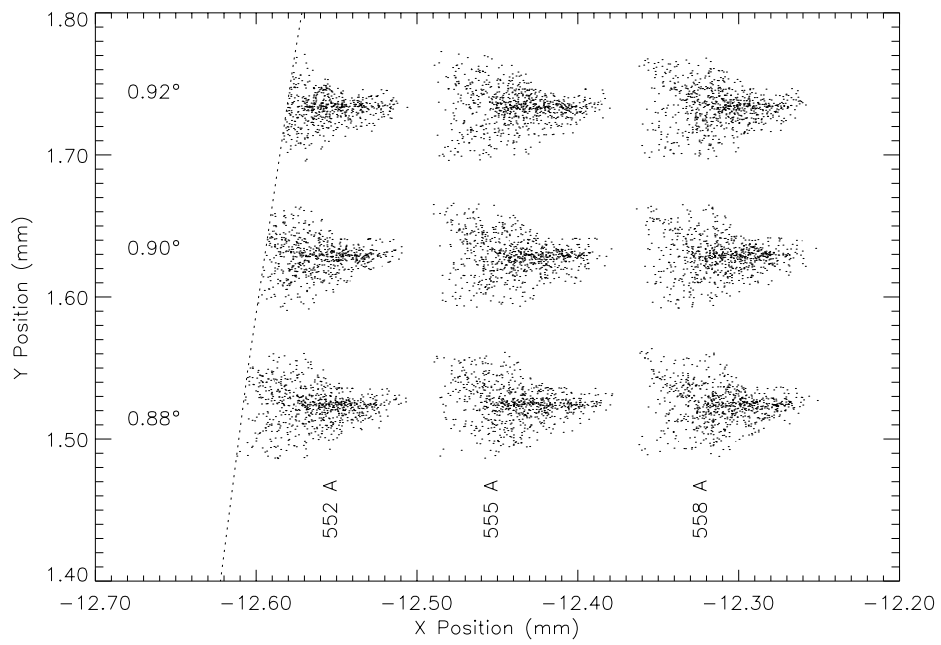


Fig. 6. A demonstration of the spatial and spectral resolution at the edge of the bandpass and the edge of the FOV. The dotted line to the left is the edge of the hypothetical detector.

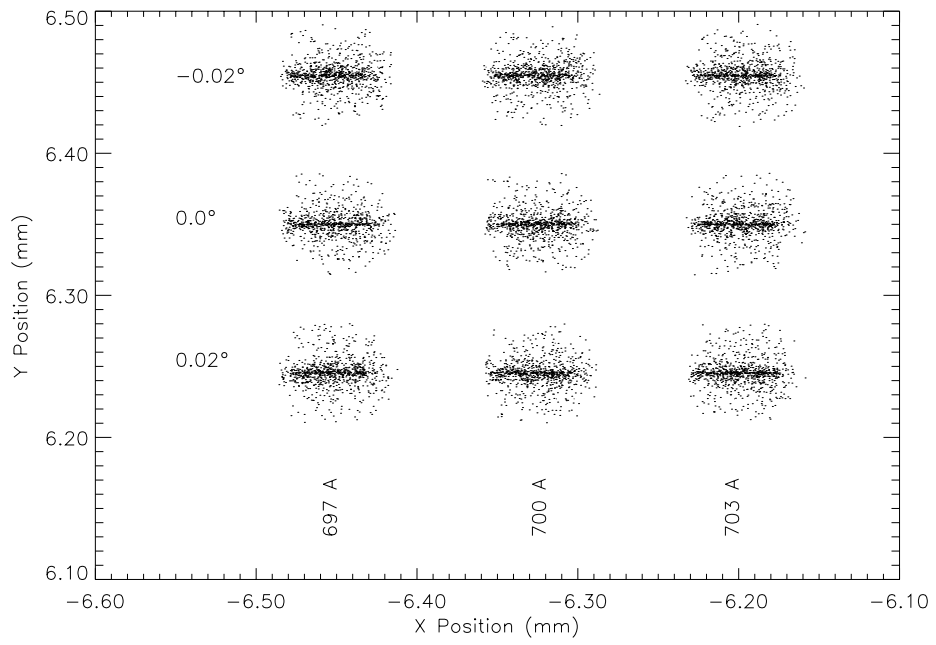


Fig. 7. A demonstration of the spatial and spectral resolution at the best focus wavelength in the center of the FOV.

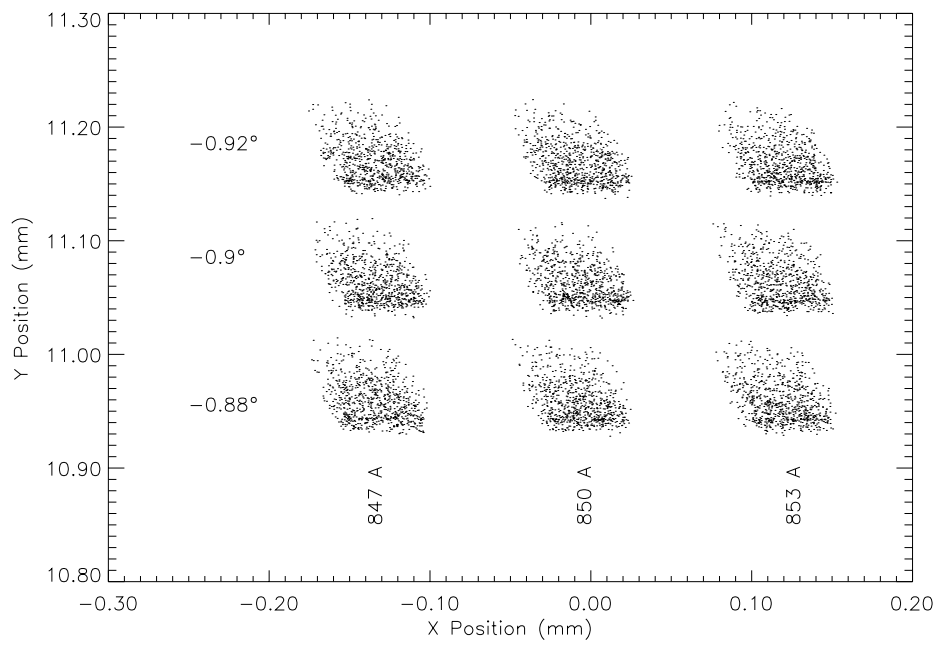


Fig. 8. A demonstration of the spatial and spectral resolution at the center of the bandpass and the edge of the FOV.

## List of Tables

1	Instrument parameters for the solar and planetary SEIS . . . . .	19
---	--	----

Table 1. Instrument parameters for the solar and planetary SEIS

Feature	Parameter	
	Solar	Planetary
Resolution:	9.5Å	2.0Å
Bandpass:	300–1310Å	550–1100Å
Field of View:	2.5 × 2.5°	6.6 × 1.8°
Slit Size:	0.080 mm × 1 mm	0.50 mm × 35 mm
Incidence Angle:	5°	4.55°
Grating:		
Line Density:	850/mm	1400/mm
Blank Size:	20 mm × 20 mm	40 mm × 40 mm
Ruled Area:	15 mm × 15 mm	35 mm × 35 mm
Radius of Curvature:	200 mm × 400 mm	300 mm × 600 mm
Blaze Wavelength:	200Å	800Å
Reflective Coating:	Au	SiC
Detector:		
Type	MCP w/wedge-strip readout	MCP w/wedge-strip readout
Photocathode	none	KBr
Resolution	0.1 mm square	0.05 mm square